

Optimum design of hierarchical stiffened shells for low imperfection sensitivity

Bo Wang · Peng Hao · Gang Li · Jia-Xin Zhang · Kai-Fan Du · Kuo Tian · Xiao-Jun Wang · Xiao-Han Tang

Received: 17 September 2013 / Revised: 2 November 2013 / Accepted: 28 November 2013

©The Chinese Society of Theoretical and Applied Mechanics and Springer-Verlag Berlin Heidelberg 2014

Abstract A concept of hierarchical stiffened shell is proposed in this study, aiming at reducing the imperfection sensitivity without adding additional weight. Hierarchical stiffened shell is composed of major stiffeners and minor stiffeners, and the minor stiffeners are generally distributed between adjacent major stiffeners. For various types of geometric imperfections, e.g., eigenmode-shape imperfections, hierarchical stiffened shell shows significantly low imperfection sensitivity compared to traditional stiffened shell. Furthermore, a surrogate-based optimization framework is proposed to search for the hierarchical optimum design. Then, two optimum designs based on two different optimization objectives (including the critical buckling load and the weighted sum of collapse loads of geometrically imperfect shells with small- and large-amplitude imperfections) are compared and discussed in detail. The illustrative example demonstrates the inherent superiority of hierarchical stiffened shells in resisting imperfections and the effectiveness of the proposed framework. Moreover, the decrease of imperfection sensitivity can finally be converted into a decrease of structural weight, which is particularly important in the development of large-diameter launch vehicles.

The project was supported by the National Basic Research Program of China (2014CB049000, 2014CB046506), the Project funded by China Postdoctoral Science Foundation (2014M551070), the National Natural Science Foundation of China (11372062, 91216201, 11128205), the Fundamental Research Funds for the Central Universities (DUT14RC(3)028) and the LNET Program (LJQ2013005).

B. Wang · P. Hao · G. Li (✉) · J.-X. Zhang · K.-F. Du · K. Tian
State Key Laboratory of Structural Analysis for
Industrial Equipment,
Department of Engineering Mechanics,
Dalian University of Technology, 116023 Dalian, China
e-mail: ligang@dlut.edu.cn
X.-J. Wang · X.-H. Tang
Beijing Institute of Astronautical Systems Engineering,
100076 Beijing, China

Keywords Hierarchical stiffened shell · Imperfection sensitivity · Collapse · Optimization

1 Introduction

Stiffened shells have been one of the primary structural elements for constructing a large-diameter launch vehicle. For these thin-walled structures under axial compression, buckling is the main failure mechanism, which can generally be categorized as skin buckling, rib crippling and global collapse [1]. Collapse load is a governing assessment of load-carrying capacity obtained by a nonlinear post-buckling analysis accounting for both geometric and material nonlinearities, which is specified by that point of the load-shortening curve where a sharp decrease occurs, thus limiting the load-carrying capacity [2].

Due to the axial compression loads caused by ascent, launch vehicle shell structures generally require lightweight designs with high specific bending stiffness to resist buckling and collapse. Buckling optimization of stiffened shells under axial compression remains a subject of active research, with special emphasis laid on finding the minimum weight or (and) maximum performance designs [3–5], since launch vehicle structures consist mostly of stiffened panels or shells. In order to reduce the computational burden caused by large number of iterations, surrogate models have been successfully adopted in the optimization of stiffened panels and shells [6, 7]. Also, Hao et al. [8] developed a bi-step surrogate-based optimization framework with adaptive sampling to obtain the optimum design for non-uniform stiffened shells. Besides, a concept of stiffened panel with varying stiffener sizes was developed to improve the local stability and in turn the static strength performance [9, 10]. Then the concept of sub-stiffened shells was intensively promoted and integrated into PANDA2 by Bushnell and Rankin [9], and the experimental validation was then carried out by Quinn et al. [10].

However, extensive work has proven that initial geometrical imperfections can drastically reduce the load-carrying capacity of stiffened shells compared to that of geometrically perfect structures [11–13]. With the advent of Chinese newly developed and future heavy-lift launch vehicles, diameter of the core stage increases from 3.35 m to 5 m, then to 9 m, however, the equivalent thickness increases only to a small extent due to the weight limit of launch vehicles. The increase of R/t (ratio of shell radius to equivalent thickness) leads to the fact that the effects of initial imperfections on the load-carrying capacity of stiffened shells become more significant, which results in an extremely high imperfection sensitivity, as indicated in the guideline from NASA [14]. Among various types of imperfections, eigenmode-shape imperfection is the most commonly adopted one at the design stage [15]. The European standard for steel shell structures recommends that the imperfection should be specified in the form of eigenmode shape, with its amplitude linked to fabrication quality, unless a different unfavourable pattern is justified [16].

Most of the previous works focused on the sensitivity of classical stiffened shells to various types of imperfections, rather than aiming at decreasing the imperfection sensitivity of structural designs [15–17]. Experimental results showed that shells with equal buckling load for the perfect shell may have different buckling loads for imperfect shells [18]. Further, it should be emphasized that a decrease of imperfection sensitivity is usually converted into a decrease in structural weight, which is particularly important in the development of large-diameter launch vehicles. On this account, Wang et al. [19] compared the eigenmode-shape imperfection sensitivity of three types of stiffened shells with practically the same structural weights, and it was found that the orthogrid stiffened shell is a more robust design choice compared to the isogrid one.

Obviously, it is worthwhile to develop more sensible design methods to reduce the imperfection sensitivity, such as optimization methods. In fact, a design can be named “optimal” only if the influence of imperfections and the resulting decrease of the load-carrying capacity are added to the design criteria [20]. However, only limited work has been done until now on the optimization of stiffened shells with imperfection sensitivity taken into account [21]. Hao et al. [22] proposed a concept of stiffened shell with outward hyperbolic generatrix shape to resist the reduction of load-carrying capacity caused by imperfections, and an optimization framework including load-carrying capacity and imperfection sensitivity for stiffened shells was presented to find a robust design.

In this study, a concept of hierarchical stiffened shell is proposed, aiming at reducing the imperfection sensitivity without adding additional weight. For various types of geometric imperfections, e.g., eigenmode-shape imperfections, hierarchical stiffened shells show significantly low imperfection sensitivity compared to traditional stiffened shells. Fur-

thermore, a surrogate-based optimization framework is proposed to find the hierarchical optimum design. Then two optimum designs based on two different optimization objectives are compared and discussed. Specifically, the first objective is the critical buckling load of perfect stiffened shell, and the other is the nominal collapse load accounting for the load-carrying capacities of stiffened shells with small- and large-amplitude imperfections. The illustrative example demonstrates the inherent superiority of hierarchical stiffened shells and the effectiveness of the proposed framework.

2 Methodology

2.1 Explicit dynamic analysis

Nonlinear explicit dynamic analysis allows to investigate the deformed shape evolution of stiffened panels from pre-buckling to post-buckling until global collapse occurs.

The equation of motion for a structure can be expressed as

$$\left(\frac{\mathbf{M}}{\Delta t^2} + \frac{\mathbf{C}}{2\Delta t}\right)\mathbf{U}_{t+\Delta t} = \mathbf{F}_t^{\text{ext}} - \mathbf{F}_t^{\text{int}} + \left(\frac{2\mathbf{M}}{\Delta t^2} - \mathbf{K}\right)\mathbf{U}_t - \left(\frac{\mathbf{M}}{\Delta t^2} - \frac{\mathbf{C}}{2\Delta t}\right)\mathbf{U}_{t-\Delta t}, \quad (1)$$

where \mathbf{M} is the mass matrix, \mathbf{C} is the damping matrix, \mathbf{K} is the stiffness matrix, \mathbf{U} is the vector of nodal displacement, t is the time, Δt is the time increment, $\mathbf{F}_t^{\text{ext}}$ is the vector of applied external force, $\mathbf{F}_t^{\text{int}}$ is the vector of internal force. Referring to Eq. (1), it can be seen that $\mathbf{U}_{t+\Delta t}$ depends on \mathbf{U}_t and $\mathbf{U}_{t-\Delta t}$. Consequently, the equations can be solved directly, and no convergence checks are needed since the equations are uncoupled.

Explicit dynamic analysis can provide accurate and robust predictions on post-buckling behavior and collapse load of stiffened panels, which was proved to be in fairly good agreement with experimental results [23].

2.2 Representation of geometrical imperfections

In practice, various forms of imperfections can be caused by manufacturing, transport, installation and serving processes of stiffened shells. It has been generally recognized that initial geometrical imperfections are a major contributor to the discrepancy between the predicted collapse loads and the experimentally measured ones. Geometry of an imperfect stiffened shell can be defined by

$$\mathbf{X} = \mathbf{X}_p + \mathbf{X}_{\text{imp}}, \quad (2)$$

$$\mathbf{X}_{\text{imp}} = \delta \mathbf{N}, \quad (3)$$

$$\alpha = \delta / (h + t_s), \quad (4)$$

where \mathbf{X}_p is the nodal coordinates vector of perfect geometry, \mathbf{X}_{imp} is the nodal displacement vector caused by imperfections, representing deviations from the perfect geometry, δ is the maximal amplitude of the deviations along the radial direction, α is the non-dimensional imperfection amplitude, \mathbf{N} is the nodal coordinates vector of the base imperfection

shape, which can be chosen arbitrarily, such as in the forms of eigenmode, dimple, out-of-roundness, out-of-straight, hyperbolic shapes, h is the stiffener height, and t_s is the skin thickness.

3 Post-buckling and imperfection sensitivity analyses

3.1 Description of the initial design

A 3m-diameter orthogrid stiffened shell is investigated in this study, which can be considered to be representative of the fuel tanks in modern launch vehicles. The orthogrid stiffener pattern and design variables are shown in Fig. 1. The initial values of the geometrical parameters are provided in Table 1. Typical properties of the aluminum alloy used for this study are as follows: Young's modulus $E = 70$ GPa, Poisson's ratio $\nu = 0.33$, yield stress $\sigma_s = 410$ MPa, ultimate stress $\sigma_b = 480$ MPa, density $\rho = 2.7$ t/m³.

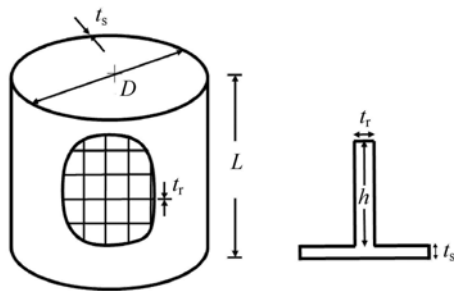


Fig. 1 Schematic of the orthogrid stiffened shell

Table 1 Values of the geometrical parameters for the traditional stiffened shell

Item	Value
Diameter D /m	3.0
Length L /m	2.0
Skin thickness t_s /mm	4.0
Stiffener thickness t_r /mm	9.0
Stiffener height h /mm	15.0
Number of circumferential stiffeners N_c	25
Number of axial stiffeners N_a	90

The general-purpose code ABAQUS is employed to establish the finite element model of stiffened shell using the S4R element (shell element with 4 nodes and reduced numerical integration) with six degrees of freedom at each node. According to the preliminary analysis, lower computational time can be achieved using S4R element with the accuracy only slightly affected [24]. The lower end of the stiffened shell is clamped, while the upper end fixes all the degrees of freedom except for the axial displacement. A uniform axial displacement is imposed to the upper end of the stiffened shell. In an explicit dynamic analysis, for each load step, axial load is calculated by summing the reaction loads of the

nodes at the lower end. Eventually, the collapse load of stiffened shell is specified by that point of the load-shortening curve where a sharp decrease occurs, thus limiting the load-carrying capacity.

Dependence analysis of element size for the stiffened shell model is firstly performed. Taking the computational cost into account, the number of elements along the direction of stiffener height is chosen as 2, and the mesh size of the skin is selected as 30 mm. The critical buckling load obtained by a linear buckling analysis is 13 542 kN, with the buckling mode shown in Fig. 2, where U is the radial displacement in mm. The predicted collapse load obtained by a nonlinear explicit dynamic analysis is 16 853 kN, and the predicted deformed shape at the collapse load is also shown in Fig. 3.

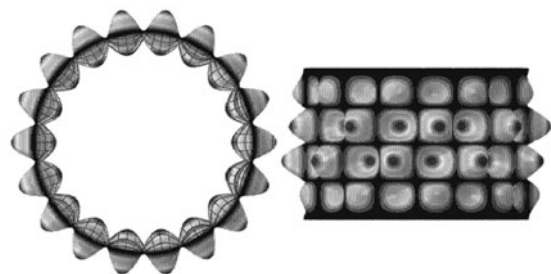


Fig. 2 Buckling mode of the traditional stiffened shell

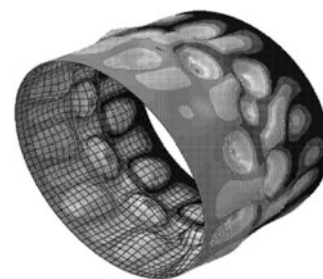


Fig. 3 Deformed shape of the traditional stiffened shell at the collapse load (scaled by 5.0)

3.2 Imperfection sensitivity analysis of traditional stiffened shell

At the preliminary design stage of stiffened shells, detailed information on both the form and amplitude of the real imperfections is not known a priori due to the lack of experimental data. Thus eigenmode-shape imperfection is recommended to be utilized in such cases, although these obtained results are expected to be conservative because the eigenmode-shape imperfection represents the deformation shape which is prone to buckling [16].

The eigenmode-shape imperfection sensitivity curve of the traditional stiffened shell is shown in Fig. 4, together with the deformed shapes at the collapse loads. In this study, the range of concerned non-dimensional imperfection amplitude

is specified as $[0.0, 1.0]$ (for the case of $\alpha = 1.0$, the absolute imperfection amplitude equals to the sum of stiffener height and skin thickness), which is assumed to be sufficient to include a practical range of imperfection amplitudes that would be acceptable for as-built cylinders [25]. Initially, the collapse load decreases sharply with the increase of the imperfection amplitude. When $\delta > 9.5$ mm ($\alpha > 0.5$), the collapse load almost does not decrease with further increasing δ . Finally, the lower bound of this curve $P_{co} = 7954$ kN is reached at $\delta = 19.0$ mm ($\alpha = 1.0$). Also, the evolution of deformed shapes indicates the change of post-buckling equilibrium path with the increase of imperfection amplitude.

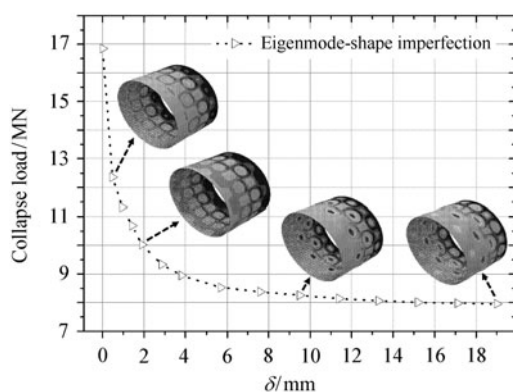


Fig. 4 Eigenmode-shape imperfection sensitivity curve of the traditional stiffened shell (scaled by 10.0)

3.3 Imperfection sensitivity analysis of hierarchical stiffened shell

In this section, a hierarchical stiffened shell is established based on the traditional one described in Sect. 3.1, as shown in Fig. 5. The structural weights of two models are identical, and the values of the geometrical parameters are listed in Table 2, where the subscripts “j” and “n” represent the major and the minor stiffeners, respectively. The other parameters are identical with the traditional one. In particular, the heights of the circumferential stiffeners at both ends of the shell are set as h_j , while the widths take a value of t_m .

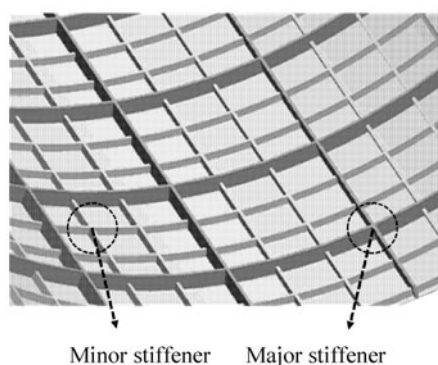


Fig. 5 Schematic of the hierarchical orthogrid stiffened shell

The critical buckling load obtained by a linear buckling analysis is 14 790 kN, with the buckling mode shown in Fig. 6. The predicted collapse load obtained by a nonlinear explicit dynamic analysis is 17 265 kN, and the predicted deformed shape at the collapse load is shown in Fig. 7.

Table 2 Values of the geometrical parameters for the hierarchical stiffened shell

Item	Value
Major stiffener thickness t_{ij} /mm	9.0
Minor stiffener thickness t_m /mm	9.0
Major stiffener height h_j /mm	23.0
Minor stiffener height h_n /mm	11.5
Number of circumferential major stiffeners N_{cj}	7
Number of circumferential minor stiffeners N_{cn}	18
Number of axial major stiffeners N_{aj}	30
Number of axial minor stiffeners N_{an}	60

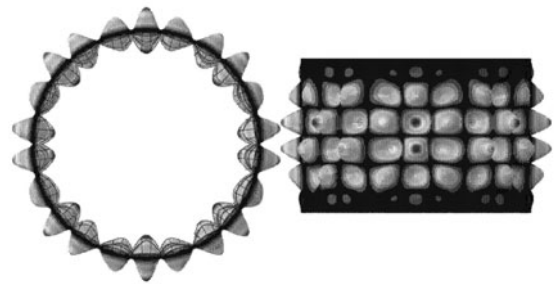


Fig. 6 Buckling mode of the hierarchical stiffened shell

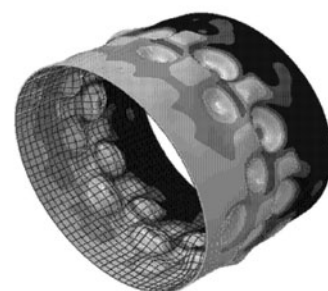


Fig. 7 Deformed shape of the hierarchical stiffened shell at the collapse load (scaled by 5.0)

Then, the eigenmode-shape imperfection sensitivity analysis is carried out for the hierarchical stiffened shell, as shown in Fig. 8. It is evident that the collapse loads of imperfect hierarchical stiffened shells are significantly higher than those ones of imperfect traditional stiffened shells, although the collapse loads of two types of perfect stiffened shells are almost the same. On this account, the hierarchical stiffened pattern may be considered as an alternative approach to reduce the imperfection sensitivity of structures.

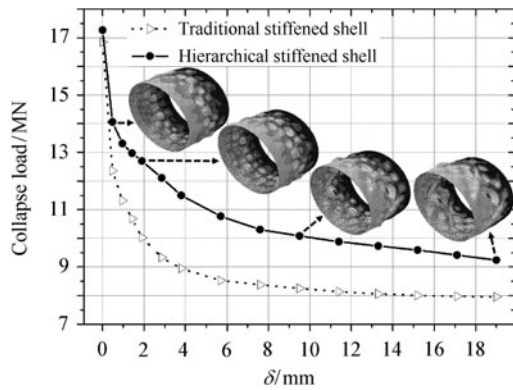


Fig. 8 Eigenmode-shape imperfection sensitivity curve of the hierarchical stiffened shell (scaled by 10.0)

To explain this phenomenon, typical eigenmode-shape imperfections are selected ($\delta = 1.9$ mm), and load vs. end-shortening curves of traditional and hierarchical stiffened shells with such imperfections are given in Fig. 9. Then, the deformed shapes of two stiffened shells with various typical end-shortenings (each end-shortening U_e is assigned with a case number) are listed in Table 3, and the magnifications of the deformations are given in Table 4, with the case numbers marked in Fig. 9. As can be seen, the collapses of traditional and hierarchical stiffened shells occur at case 3 and 6, respectively (corresponding to $U_e = 6.5$ mm and $U_e = 8.0$ mm).

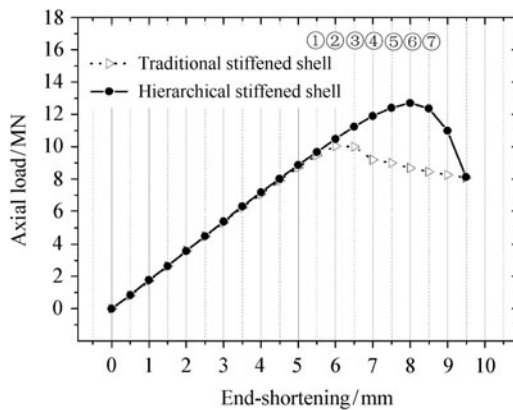


Fig. 9 Load vs. end-shortening curves of traditional and hierarchical stiffened shells with eigenmode-shape imperfections

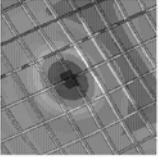
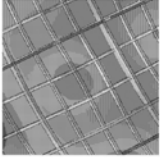
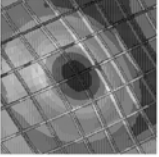
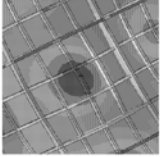
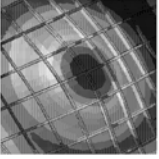
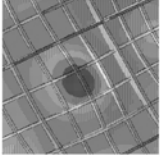
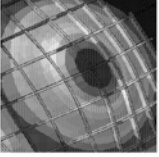
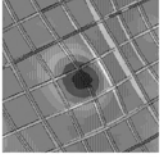
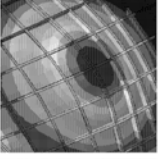
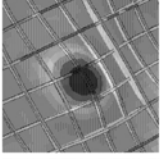
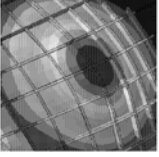
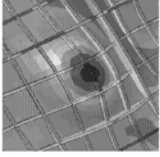
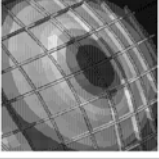

As can be observed from Tables 3 and 4, the developments of the out-of-plane deformations of hierarchical stiffened shell are restricted, compared to the ones of traditional stiffened shell. Specifically, it is evident that the out-of-plane deformations of hierarchical stiffened shell are smaller than the ones of traditional stiffened shell with the same end-shortening, until the collapse loads of two shells are reached. This may be attributed to the increase of the non-uniform stiffness of structures along the axial and circumferential directions caused by the hierarchical stiffened pattern. The

essence of geometrical imperfections is the superposition of a small/large number of local out-of-plane deformations with various forms, which may accelerate the developments of local deformations to global deformations with the increase of axial compression, and thus result in a reduction of load-carrying capacity. Obviously, the existence of major stiffeners in hierarchical stiffened shell has the ability to restrict the development of the initial deformation, therefore the imperfection sensitivity is reduced.

Table 3 Comparison of deformed shapes of traditional and hierarchical stiffened shells with eigenmode-shape imperfections

Traditional stiffened shell	Hierarchical stiffened shell

Table 4 Magnifications of deformed shapes of traditional and hierarchical stiffened shells with eigenmode-shape imperfections (scaled by 5.0)

Traditional stiffened shell	Hierarchical stiffened shell
	
	
	
	
	
	
	

In addition, from the manufacturing viewpoint, hierarchical stiffened shell is convenient to fabricate by numerical control milling, and this further enhances the benefits of the hierarchical stiffened shell.

4 Optimization framework of hierarchical stiffened shells for low imperfection sensitivity

4.1 Linear buckling optimization of hierarchical stiffened shell

Aerospace industry increasingly relies on the use of lightweight structures to meet financial and environmental targets. Firstly, linear buckling optimization is carried out,

and this is based on the consideration that the trend of critical buckling load substantially accords with the one of collapse load, however, the computing cost for obtaining critical buckling load is relatively small compared to that for collapse load. The optimization formulation by means of linear buckling analysis can be expressed as

$$\text{Maximize: } P_{cr} \quad (5)$$

$$\text{Subject to: } W \leq W_0 \quad (6)$$

$$X_i^l \leq X_i \leq X_i^u, \quad i = 1, 2, \dots, 9, \quad (7)$$

where P_{cr} is the critical buckling load of the hierarchical stiffened shell (obtained by a linear buckling analysis), W_0 is the weight of the initial design, X_i is the i -th design variable, X_i^l and X_i^u are the lower and upper bounds of the i -th design variable, as listed in Table 5. In this study, two types of variables N_{cj} (N_{aj}) and m_c (m_a) are involved: N_{cj} (N_{aj}) is the total number of circumferential (axial) major stiffeners, m_c (m_a) is the number of circumferential (axial) minor stiffeners between two adjacent major stiffeners (ranges from 1 to 4). For the circumferential stiffeners, $(N_{cj} - 1)m_c$ is the total number of minor stiffeners. For the axial stiffeners, $(N_{aj} - 1)m_a$ is the total number of minor stiffeners. N_{cj} (N_{aj}) and m_c (m_a) are two integers, thus the number of major stiffeners could be an arbitrary integer between lower and upper bounds, while the number of minor stiffeners could only be several discrete integers between lower and upper bounds.

Table 5 Design space of the variables in the hierarchical stiffened shell

Item	Initial design	Lower bound	Upper bound
t_s/mm	4.0	2.5	5.5
t_{ij}/mm	9.0	6.0	12.0
t_m/mm	9.0	6.0	12.0
h_j/mm	23.0	15.0	23.0
h_n/mm	11.5	9.0	15.0
N_{cj}	7	4	10
N_{cn}	18	3	36
N_{aj}	30	20	50
N_{an}	60	20	200

Since the buckling and post-buckling analyses of stiffened shells are time-consuming, surrogate-based optimization technology is adopted in this study. Typically, a surrogate-based optimization can be decomposed into inner optimization and outer update, as shown in Fig. 10. Actually, the inner optimization is entirely based on the surrogate model and needs negligible computational cost. The optimization is considered to be converged if the relative error between the results obtained from the surrogate model and the ones from exact finite element analysis (FEA) is less than 0.1%, otherwise the surrogate model is updated

by exact FEA (refitting the model with both old and new sampling data) and another inner optimization search is performed based on the new surrogate model. In other words, the predicted performance of the final optimum result by surrogate model has been validated by exact FEA, which can be used with full confidence.

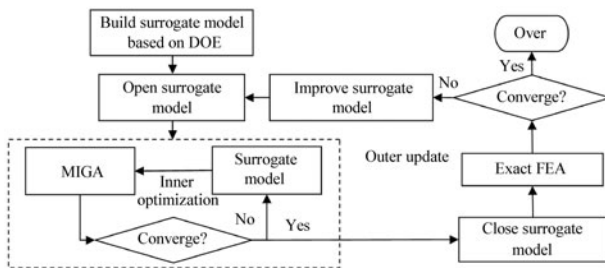


Fig. 10 Flowchart of the surrogate-based optimization

In the design of experiment (DOE), a set of 100 sampling points is generated using optimal latin hypercube sampling (OLHS) method throughout the entire design space, which is a stratified sampling approach with the restriction that each input variable has all portions of its distribution represented by input values [26]. Then radial basis function (RBF) model is constructed based on the sampling data, which was proved to be the most dependable method in most situations for global optimization in terms of accuracy and robustness [27]. To evaluate the quality of RBF model, another sample set composed of 18 sampling points is generated by OLHS. Three metrics are calculated by the sample set, including the percent root mean square error (e_{RMS}), the percent average error (e_a), and the percent maximum error (e_m) [28, 29], which are defined as

$$e_{\text{RMS}} = \sqrt{\frac{1}{n} \sum_{i=1}^n (y_i - \tilde{y}_i)^2} \left/ \left(\frac{1}{n} \sum_{i=1}^n y_i \right) \right. \quad (8)$$

$$e_a = \frac{1}{n} \sum_{i=1}^n |y_i - \tilde{y}_i| \left/ \left(\frac{1}{n} \sum_{i=1}^n y_i \right) \right. \quad (9)$$

$$e_m = \text{Max} \left[|y_i - \tilde{y}_i| \left/ \left(\frac{1}{n} \sum_{i=1}^n y_i \right) \right. \right] \quad (10)$$

where y_i is the response value at the i -th test point from the exact function, \tilde{y}_i is the prediction value from the surrogate model, n is the number of test points. The smaller the values of three error metrics, the higher the fidelity of the surrogate model.

As can be seen from Table 6, the prediction of weight is generally more accurate compared to the critical buckling load. All the e_{RMS} and e_a are under 10%, whereas the e_m is relatively large. For the prediction of P_{cr} , e_m reaches a value of 15.9%, and this is due to the fact that the RBF model could not give an accurate prediction for a design when the con-

straint is seriously violated, unless more samples surrounding this design are added to the training sample set. However, it is obvious that the optimum design would not violate the constraint, thus the prediction accuracy of RBF model for such a design is not of our concern.

Table 6 Modeling errors of the surrogate model in the linear buckling optimization

Item	$e_{\text{RMS}}/\%$	$e_a/\%$	$e_m/\%$
W	1.6	1.1	4.7
P_{cr}	6.2	4.5	15.9

Once the surrogate model is built successfully, multi-island genetic algorithm (MIGA) is adopted in the surrogate-based optimization to find the optimum design, which is a stochastic search algorithm based on the mechanics of natural selection and genetics, and thus gives the algorithm the ability to correct deterministic search bottlenecks that are caused by the reasoning in the gradient methods. In MIGA, the population in one generation is divided into several islands, and the genetic operations are performed independently on each island. This independency enables the calculation to avoid converging local optimums [30]. For the sake of clarity, iterations based on the surrogate model are removed, and only the history of outer updates is plotted in Fig. 11. Initially, the accuracy of the surrogate model is relatively low, thus the convergence curve shows somewhat oscillation. With the assistance of outer updates and new samples, the fidelity of the surrogate model is improved continuously.

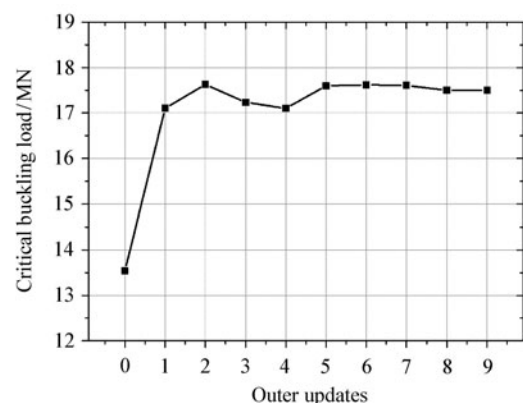


Fig. 11 History of the outer updates in the linear buckling optimization

After the evolution of 9 outer updates, the optimum design is achieved, as shown in Fig. 12. The critical buckling load obtained by a linear buckling analysis is 17 499 kN, with the buckling mode shown in Fig. 13. The collapse load obtained by a nonlinear explicit dynamic analysis is 19 813 kN,

and the predicted deformed shape at the collapse load is shown in Fig. 14. The comparison of the initial design and the optimum design is summarized in Table 7. It can be found that both the critical buckling load and collapse load have been improved to a large extent, and the mechanism may be explained as follows: the hierarchical stiffened pattern enables the major stiffeners to be long-spaced and the height of major stiffeners to take a large value to resist bending and global buckling. On the other hand, the minor stiffener could reduce the accompanied risk of local buckling.

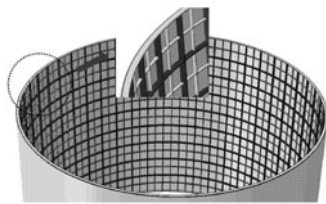


Fig. 12 Geometry of the optimum design obtained by the linear buckling optimization

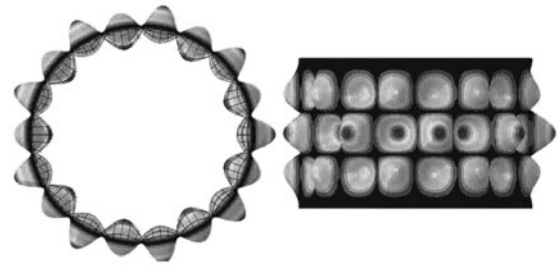


Fig. 13 Buckling mode of the optimum design obtained by the linear buckling optimization

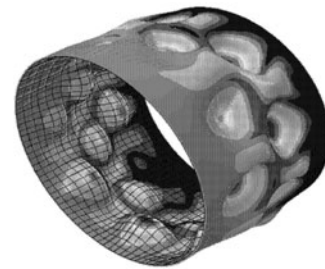


Fig. 14 Deformed shape of the optimum design obtained by the linear buckling optimization (scaled by 5.0)

Table 7 Comparison of the performances for the initial and the optimum designs

Item	Initial design (traditional)	Initial design (hierarchical)	Linear buckling optimum design	Optimum design including IS
W/kg	354.6	354.6	353.9	353.9
P_{cr}/kN	13 542	14 790	17 499	13 938
P_{co}/kN	16 853	17 265	19 813	16 920
$P_{0.1}/\text{kN}$	10 021	12 701	13 113	13 985
$P_{1.0}/\text{kN}$	7 954	9 237	8 907	10 310
P_{nom}/kN	8 988	10 969	11 010	12 148

4.2 Optimization of hierarchical stiffened shell including imperfection sensitivity (IS)

Imperfection sensitivity is always neglected in the traditional optimization of stiffened shells. However, the optimum design is usually accompanied with a large degree of imperfection sensitivity. From the viewpoint of practicality and long-term reliability, such an optimum design is inadequate and even dangerous [24]. Thus, imperfection sensitivity needs to be taken into account in this optimization. Because various geometrical imperfections can be accurately modeled into the perfect structure with the aid of modern CAE technology, detailed FEM models are employed in the following optimization.

Due to the fact that a post-buckling analysis of stiffened shell by FEM is extremely time-consuming, surrogate model is employed in this study to reduce the computational burden caused by the large number of iterations during op-

timization. For this illustrative example, the computational time of an explicit dynamic analysis of perfect or imperfect stiffened shell is about 1.8 h, using a computer with a CPU of P4 2.9 GHz and 4 G RAM.

In this section, eigenmode shape is selected as the illustrative imperfection, representing the global-pattern imperfection (composed of a large number of local out-of-plane deformations throughout the whole shell), which is commonly utilized in the evaluation of imperfection sensitivity of thin-walled structures. From a typical imperfection sensitivity curve of stiffened shells, e.g., Fig. 4, one high gradient stage ($0 < \alpha < 0.3$) and one relatively stable stage ($0.3 < \alpha < 1.0$) can be clearly observed. To accurately describe the overall imperfection sensitivity, two amplitudes of $\alpha = 0.1$ and $\alpha = 1.0$ are selected from two stages to represent the property of the whole curve. Nominal collapse load is further defined herein to evaluate both the load-carrying capacity of geometrically perfect stiffened shell and its im-

perfection sensitivity, which can be formulated as a weighted sum of collapse loads of geometrically imperfect shells with small- ($\alpha = 0.1$) and large-amplitude ($\alpha = 1.0$) imperfections, as shown in Eq. (11). Also, weight constraint is considered, and the involved variables include skin thickness t_s , stiffener width t_r , and height h , the numbers of circumferential and axial major stiffeners, N_{cj} and N_{aj} , the numbers of circumferential and axial minor stiffeners, N_{cn} and N_{an} , respectively. Specifically, the same stiffener numbers are chosen as used in the previous optimization. Hence, the formulation of this optimization problem can be stated as

$$\text{Maximize: } P_{\text{nom}} = \beta_1 P_{0.1} + \beta_2 P_{1.0}, \quad (11)$$

$$\text{Subject to: } W \leq W_0, \quad (12)$$

$$\beta_1 + \beta_2 = 1, \quad (13)$$

$$X_i^l \leq X_i \leq X_i^u, \quad i = 1, 2, \dots, 9, \quad (14)$$

where β_1 and β_2 are the weighted coefficients of two collapse loads, which are set as 0.5 for simplicity in this work. W is the weight of stiffened shell, W_0 is the weight of the initial design, X_i is the i -th design variable, X_i^l and X_i^u are the lower and upper bounds of the i -th design variable, as listed in Table 5.

Similarly, a set of 100 sampling points is firstly generated using the OLHS throughout the design space, and RBF model is constructed based on the sampling data. To evaluate the quality of RBF model, another sample set composed of 18 sampling points is generated by OLHS throughout the design space. Three metrics are calculated by the test sample set, as shown in Table 8. As can be seen, all the e_{RMS} and e_a are under 10%, where the e_m is relatively large. This may be caused by the fact that the design space has been enlarged substantially due to the presence of major stiffeners. For some extreme designs (which have extremely large or small structural weight), the accuracy of the surrogate model is low. Fortunately, these designs do not influence the exploration of the optimum design in the optimization. Besides, the prediction of structural weight is generally more accurate compared to the prediction for collapse loads, since the load-carrying capacities show higher nonlinearity with respect to the variations of variables.

Table 8 Modeling errors of the surrogate model in the optimization including IS

Item	$e_{\text{RMS}}/\%$	$e_a/\%$	$e_m/\%$
W	1.2	0.9	2.3
$P_{0.1}$	8.0	5.6	15.5
$P_{1.0}$	6.7	5.6	14.5

Iterations of the surrogate-based optimization are shown in Fig. 15. It can be seen that the objective decreases smoothly until the convergence is achieved. The nominal collapse load of the optimum design is 12 148 kN, improved by 35.2%, and the corresponding structural weight is

353.9 kg, with the geometry of the optimum design shown in Fig. 16. The buckling mode and the deformed shape of the optimum design at the collapse load are plotted in Fig. 17 and 18, respectively.

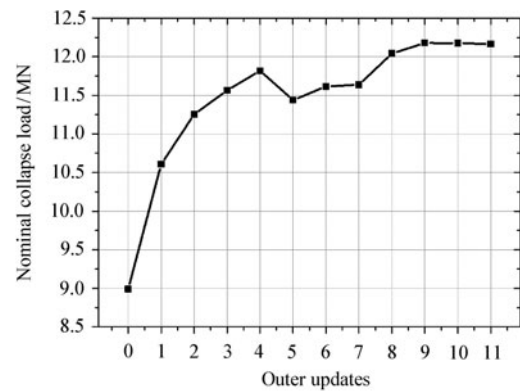


Fig. 15 History of the outer updates in the optimization including IS

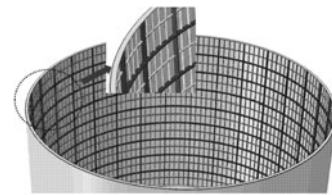


Fig. 16 Geometry of the optimum design obtained by the optimization including IS

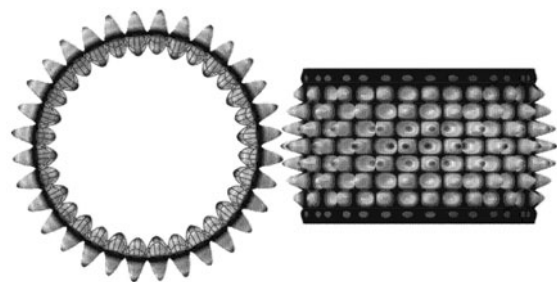


Fig. 17 Buckling mode of the optimum design obtained by the optimization including IS

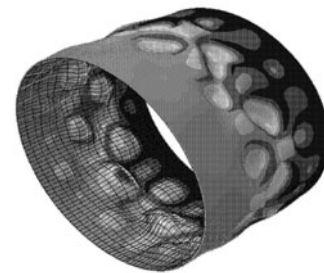


Fig. 18 Deformed shape of the optimum design at the collapse load obtained by the optimization including IS (scaled by 5.0)

4.3 Comparison of the initial and the optimum designs

For the purpose of comparison, the performances of the initial and the optimum designs are listed in Table 7, and the weights of these four designs remain practically the same. For the optimum design including IS, the critical buckling load and the collapse load of the perfect structure are improved to a small extent compared to two initial designs, while the collapse loads of the imperfect structures with small- and large-amplitudes imperfections are increased significantly. For the linear buckling optimum design, both the critical buckling load and the collapse load of the perfect structure are improved to a large extent, while the increases of collapse loads for the imperfect structures compared to the traditional initial design are not as large as the one for the perfect structure. Moreover, the collapse load of the linear buckling optimum design is even lower than that of the hierarchical initial design when $\delta = 19.0$ mm ($\alpha = 1.0$).

Further, eigenmode-shape imperfection sensitivity curves are compared for two optimum designs and the initial design, as shown in Fig. 19. Among these curves, the optimum design including IS shows higher load-carrying capacity when imperfections are taken into account, as compared to both the traditional and the hierarchical initial designs. However, for the case of $\delta > 2.85$ mm ($\alpha > 0.15$), the collapse loads in the linear buckling optimum design are even lower than the ones in the hierarchical initial design. Moreover, for sufficient small-amplitude imperfections, the performances of the linear buckling optimum design are superior to the ones of the optimum design including IS. For $\delta > 0.95$ mm ($\alpha > 0.05$), the reverse is true. Results indicate that the minimum collapse loads of the linear buckling optimum design and the optimum design including IS have been increased by 12.0% and 29.6% compared to the traditional initial design, respectively. This enhances the significance of the optimization including IS, which can provide a more robust optimum design from the viewpoint of practicality and long-term reliability.

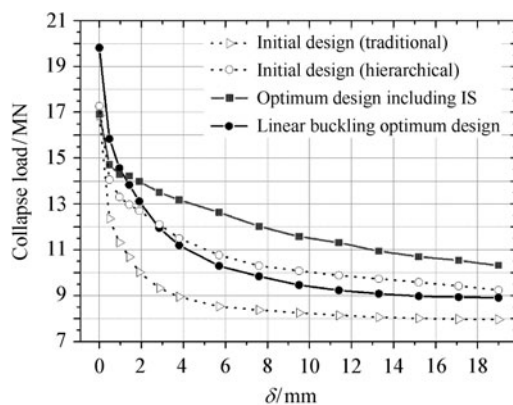


Fig. 19 Eigenmode-shape imperfection sensitivity curves of the initial and the optimum designs

Also, variable values of two optimum designs are given in Table 9. The main difference between the optimum designs of the linear buckling optimization and the optimization including IS lies in the width of major stiffeners and the numbers of axial major and minor stiffeners. To further investigate the difference between two optimum designs, load vs. end-shortening curves of two shells with eigenmode-shape imperfections of $\delta = 1.9$ mm ($\alpha = 0.1$) are shown in Fig. 20, together with several deformed shapes under various end-shortenings. As can be seen, although local buckling between adjacent major stiffeners occurs under a smaller end-shortening for the optimum design including IS ($U_e = 4.0$ mm), the shell still has the load-carrying capacity until global collapse occurs, since the major stiffeners in hierarchical stiffened shells can restrict the development of the initial out-of-plane deformations to global collapse. For a global-pattern imperfection, such as eigenmode-shape, moderate-spaced major stiffeners are expected to be able to enhance this benefit, while both close-spaced and long-spaced major stiffeners may not be suited to restrict the initial deformation.

Table 9 Comparison of the variable values of the initial and the optimum designs

Item	Initial design	Linear buckling optimum design	Optimum design including IS
t_s /mm	4.0	4.7	4.6
t_{ij} /mm	9.0	6.7	6.8
t_{rn} /mm	9.0	6.1	6.6
h_j /mm	23.0	23.0	22.6
h_n /mm	11.5	12.0	9.0
N_{cj}	7	10	10
N_{cn}	18	9	9
N_{aj}	30	50	32
N_{an}	60	50	128

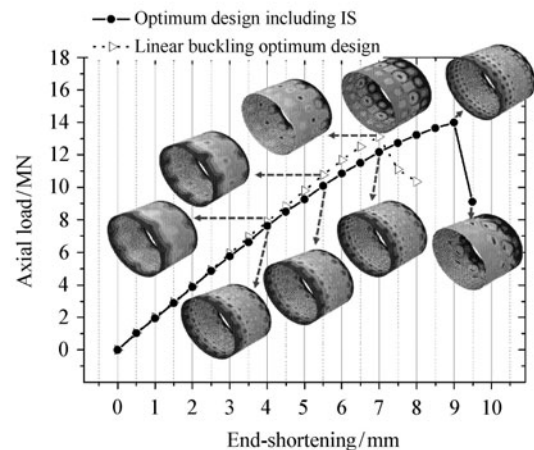


Fig. 20 Load vs. end-shortening curves of two optimum designs with eigenmode-shape imperfections

In addition, the influence of the weighted coefficients on the optimum design is another interesting subject. For the purpose of illustration, another optimization including IS is performed using two different weighted coefficients $\beta_1 = 0$ and $\beta_2 = 1.0$. As can be observed from the imperfection sensitivity curves in Fig. 21, although the collapse load of the new optimum design is slightly higher than the one of the former optimum design when $\delta = 19.0$ mm ($\alpha = 1.0$), the collapse loads of the new design are far lower than the former ones for other imperfection amplitudes, especially for small-amplitude imperfections. In this sense, it can be concluded that $\beta_1 = \beta_2 = 0.5$ has the ability to find the optimum design with a low overall imperfection sensitivity. Indeed, the specific values of these two weighted coefficients should be associated with the specific manufacturing method, which is an important subject that demands further research.

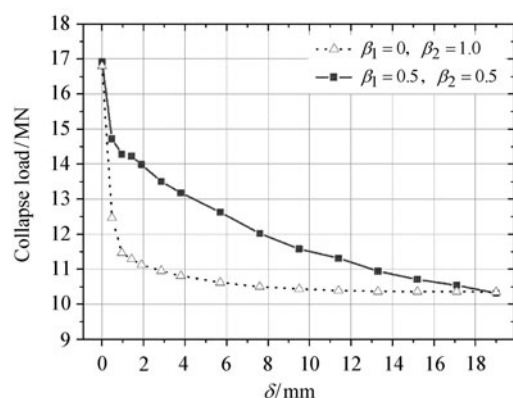


Fig. 21 Eigenmode-shape imperfection sensitivity curves of two optimum designs with different weighted coefficients

5 Conclusion

A concept of hierarchical stiffened shell is proposed in this study, aiming at reducing the imperfection sensitivity without adding additional weight.

In general, the tolerances and resistances to imperfections are increased from unstiffened shells to stiffened shells, and then to hierarchical stiffened shells. Specifically, for various types of geometric imperfections, e.g., eigenmode-shape, the hierarchical stiffened shell shows significantly low imperfection sensitivity compared to the traditional stiffened shell. This may be attributed to the increase of the non-uniform stiffness of structures along the axial and the circumferential directions. The existence of major stiffeners in hierarchical stiffened shells can restrict the development of the initial out-of-plane deformations compared to the traditional stiffened shell, therefore the imperfection sensitivity is reduced.

Furthermore, a surrogate-based optimization framework is proposed to achieve the hierarchical optimum design. Then two optimum designs based on two different optimization objectives are compared and discussed. The illus-

trative example demonstrates that the optimization formulation including imperfection sensitivity could provide a more robust design. Finally, the decrease of imperfection sensitivity can finally translate to a decrease of structural weight, which is particularly important in the development of large-diameter launch vehicles.

Acknowledgement C. Huang and L. Zhang from Beijing Institute of Astronautical Systems Engineering are much appreciated for their helpful comments and suggestions.

References

- 1 Venkataraman, S., Lamberti, L., Haftka, R.T.: Challenges in comparing numerical solutions for optimum weights of stiffened shells. *J. Spacecr Rockets* **40**, 183–192 (2003)
- 2 Degenhardt, R., Rolfes, R., Zimmermann, R., et al.: COCOMAT - improved material exploitation of composite airframe structures by accurate simulation of postbuckling and collapse. *Compos Struct.* **73**, 175–178 (2006)
- 3 Bushnell, D., Bushnell, W.D.: Minimum-weight design of a stiffened panel via PANDA2 and evaluation of the optimized panel via STAGS. *Comput Struct.* **50**, 569–602 (1994)
- 4 Leriche, R., Haftka, R.T.: Optimization of laminate stacking sequence for buckling load maximization by genetic algorithm. *AIAA J.* **31**, 951–956 (1993)
- 5 Jaunky, N., Knight, N.F., Ambur, D.R.: Optimal design of general stiffened composite circular cylinders for global buckling with strength constraints. *Compos Struct.* **41**: 243–252 (1998)
- 6 Rikards, R., Abramovich, H., Kalnins, K., et al.: Surrogate modeling in design optimization of stiffened composite shells. *Compos Struct.* **73**, 244–251 (2006)
- 7 Wu, H., Yan, Y., Yan, W., et al.: Adaptive approximation-based optimization of composite advanced grid-stiffened cylinder. *Chinese J. Aeronaut* **23**, 423–429 (2010)
- 8 Hao, P., Wang, B., Li, G.: Surrogate-based optimum design for stiffened shells with adaptive sampling. *AIAA J.* **50**, 2389–2407 (2012)
- 9 Bushnell, D., Rankin, C.: Optimum design of stiffened panels with sub-stiffeners. In: *Proc. of 46th AIAA/ASME/ASCE/AHS/ASC Structures, Structural Dynamics and Materials Conference*, Austin, TX, AIAA 2005-1932 (2005)
- 10 Quinn, D., Murphy, A., McEwan, W., et al.: Stiffened panel stability behaviour and performance gains with plate prismatic sub-stiffening. *Thin-Walled Struct.* **47**, 1457–1468 (2009)
- 11 Arbocz, J., Starnes, J.H.: Future directions and challenges in shell stability analysis. *Thin-Walled Struct.* **40**, 729–754 (2002)
- 12 Lindgaard, E., Lund, E., Rasmussen, K.: Nonlinear buckling optimization of composite structures considering “worst” shape imperfections. *Int J. Solids Struct.* **47**, 3186–3202 (2010)
- 13 Wang, B., Hao, P., Li, G., et al.: Determination of realistic worst imperfection for cylindrical shells using optimization algorithm. *Struct. Multidiscip. Optim.* **48**, 777–794 (2013)
- 14 Anonymous.: Buckling of thin-walled circular cylinders. NASA space vehicle design criteria. NASA SP-8007 (1968)
- 15 Teng, J.G., Song, C.Y.: Numerical models for nonlinear analysis of elastic shells with eigenmode-affine imperfections. *Int J.*

- Solids Struct. **38**, 3263–3280 (2001)
- 16 Anonymous.: Design of steel structures, Part 1.6: General rules-supplementary rules for the strength and stability of shell structures. Eurocode **3** (1999)
 - 17 Hilburger, M.W., Starnes, J.H.: Effects of imperfections of the buckling response of composite shells. Thin-Walled Struct. **42**, 369–397 (2004)
 - 18 Hühne, C., Rolfes, R., Breitbach, E., et al.: Robust design of composite cylindrical shells under axial compression-Simulation and validation. Thin-Walled Struct. **46**, 947–962 (2008)
 - 19 Wang, B., Hao, P., Du, K.F., et al.: Knockdown factor based on imperfection sensitivity analysis for stiffened shells. Int J. Aerosp Lightweight Struct. **1**, 315–333 (2011)
 - 20 Reitinger, R., Ramm, E.: Buckling and imperfection sensitivity in the optimization of shell structures. Thin-Walled Struct. **23**, 159–177 (1995)
 - 21 Bushnell, D., Rankin, C.: Difficulties in optimization of imperfect stiffened cylindrical shells. In: Proc. of 47th AIAA/ASME/ASCE/AHS/ASC Structures, Structural Dynamics and Materials Conference, Newport, RI, AIAA 2006-1943 (2006)
 - 22 Hao, P., Wang, B., Li, G., et al.: Surrogate-based optimization of stiffened shells including load-carrying capacity and imperfection sensitivity. Thin-Walled Struct. **72**, 164–174 (2013)
 - 23 Lanzi, L., Giavotto, V.: Post-buckling optimization of composite stiffened panels: computations and experiments. Compos Struct. **73**, 208–220 (2006)
 - 24 Paulo, R.M.F., Teixeira-Dias, F., Valente, R.A.F.: Numerical simulation of aluminium stiffened panels subjected to axial compression: Sensitivity analyses to initial geometrical imperfections and material properties. Thin-Walled Struct. **62**, 65–74 (2013)
 - 25 Haynie, W.T., Hilburger, M.W.: Comparison of methods to predict lower bound buckling loads of cylinders under axial compression. In: Proc. of 51st AIAA/ASME/ASCE/AHS/ASC Structures, Structural Dynamics and Materials Conf., Orlando, FL, AIAA 2010-2532 (2010)
 - 26 Park, J.S.: Optimal Latin-hypercube designs for computer experiments. J. Stat. Plan. Infer. **39**, 95–111 (1994)
 - 27 Jin, R., Chen, W., Simpson, T.W.: Comparative studies of meta-modelling techniques under multiple modelling criteria. Struct. Multidisc. Optim. **23**, 1–13 (2001)
 - 28 Venter, G., Haftka, R.T., Chirehdast, M.: Response surface approximations for fatigue life prediction. In: Proc. of 38th AIAA/ASME/AHS/ASC Structures, Structural Dynamic, and Materials Conf., Kissimmee, FL, AIAA-1997-1331 (1997)
 - 29 Goel, T., Haftka, R.T., Shyy, W.: Comparing error estimation measures for polynomial and kriging approximation of noise-free functions. Struct. Multidisc. Optim. **38**, 429–442 (2009)
 - 30 Reiko, T.: Distributed genetic algorithms. In: Proceedings of 3rd ICGA (1989)